



Citation for published version:

Lennox, M & Düren, T 2016, 'Understanding the kinetic and thermodynamic origins of xylene separation in UiO-66(Zr) via molecular simulation', *Journal of Physical Chemistry C*, vol. 120, no. 33, pp. 18651-18658.
<https://doi.org/10.1021/acs.jpcc.6b06148>

DOI:

[10.1021/acs.jpcc.6b06148](https://doi.org/10.1021/acs.jpcc.6b06148)

Publication date:

2016

Document Version

Peer reviewed version

[Link to publication](#)

This document is the Accepted Manuscript version of a Published Work that appeared in final form in *Journal of Physical Chemistry C*, copyright © American Chemical Society after peer review and technical editing by the publisher. To access the final edited and published work see DOI: 10.1021/acs.jpcc.6b06148.

University of Bath

Alternative formats

If you require this document in an alternative format, please contact:
openaccess@bath.ac.uk

General rights

Copyright and moral rights for the publications made accessible in the public portal are retained by the authors and/or other copyright owners and it is a condition of accessing publications that users recognise and abide by the legal requirements associated with these rights.

Take down policy

If you believe that this document breaches copyright please contact us providing details, and we will remove access to the work immediately and investigate your claim.

This document is confidential and is proprietary to the American Chemical Society and its authors. Do not copy or disclose without written permission. If you have received this item in error, notify the sender and delete all copies.

Understanding the Kinetic and Thermodynamic Origins of Xylene Separation in UiO-66(Zr) via Molecular Simulation

Journal:	<i>The Journal of Physical Chemistry</i>
Manuscript ID	jp-2016-06148r.R1
Manuscript Type:	Article
Date Submitted by the Author:	n/a
Complete List of Authors:	Lennox, Matthew; Univeristy of Nottingham, School of Chemistry Düren, Tina; University of Bath, Chemical Engineering

SCHOLARONE™
Manuscripts

Understanding the Kinetic and Thermodynamic Origins of Xylene Separation in UiO-66(Zr) via Molecular Simulation

Matthew J. Lennox[†] and Tina Düren^{§}*

[†] School of Chemistry, University of Nottingham, Nottingham, UK, NG7 2RD

[§] Department of Chemical Engineering, University of Bath, Bath, UK, BA2 7AY

ABSTRACT

Xylene isomers are precursors in many important chemical processes, yet their separation via crystallization or distillation is energy intensive. Adsorption presents an attractive, lower-energy alternative and the discovery of adsorbents which outperform the current state-of-the-art zeolitic materials represents one of the key challenges in materials design, with metal-organic frameworks receiving particular attention. One of the most well-studied systems in this context is UiO-66(Zr), which selectively adsorbs *ortho*-xylene over the other C8 alkylaromatics. The mechanism behind this separation has remained unclear, however. In this work, we employ a wide range of computational techniques to explore both the equilibrium and dynamic behavior of the xylene isomers in UiO-66(Zr). In addition to correctly predicting the experimentally-observed *ortho*-selectivity, we demonstrate that the equilibrium selectivity is based upon the complete encapsulation of *ortho*-xylene within the pores of the framework. Furthermore the

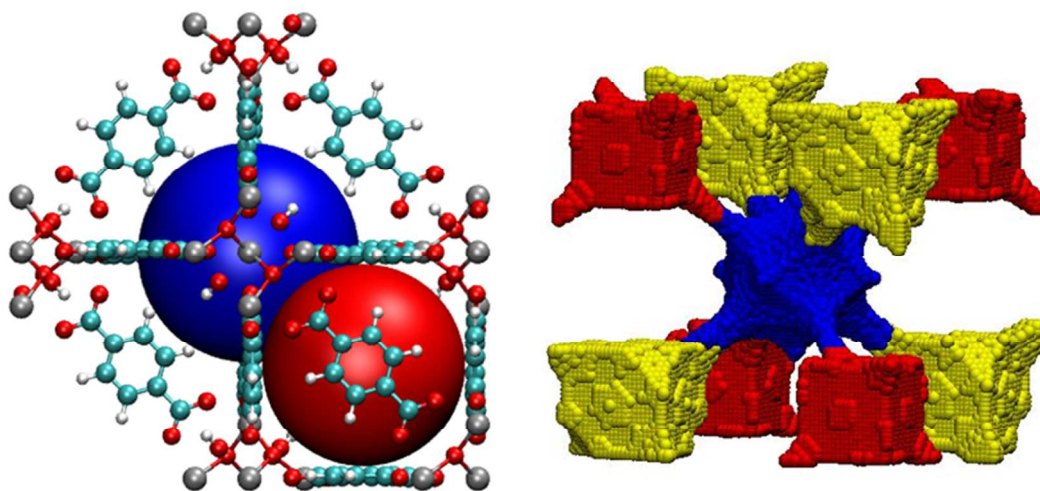
flexible nature of the adsorbent is crucial in facilitating xylene diffusion and our simulations reveal for the first time significant differences between the intracrystalline diffusion mechanisms of the three isomers resulting in a kinetic contribution to the selectivity. Consequently it is important to include both equilibrium and kinetic effects when screening MOFs for xylene separations.

INTRODUCTION

In a recent Nature contribution¹, the separation of benzene derivatives and especially xylene isomers was highlighted as one of seven separation processes “to change the world”. Xylenes (*para*-, *ortho*- and *meta*-xylene) are di-methyl-substituted aromatic compounds and are necessary precursors in a wide range of chemical processes. Of the isomers, *para*-xylene (pX) is the most important and used, for example, in the production of polymers such as PET and polyester. The efficient separation of mixtures of xylene isomers into their individual components and the recovery of *para*-xylene is therefore of great industrial relevance². The majority of pX is produced through adsorption-based separation processes typically using a simulated moving bed (SMB) and a pX-selective, ion-exchanged MFI or FAU zeolite as the adsorbent²⁻³. The efficiency of an SMB for xylene separation depends strongly upon the selectivity and capacity of the adsorbent – the development of more highly pX-selective materials would result in smaller SMB units and lower eluent consumption. Alternatively, a highly *ortho*-selective material in which pX is the least preferred isomer would not only allow the recovery of pX in the raffinate, but also the challenging downstream *ortho*-/*meta*-xylene separation to be avoided⁴. Recently, several metal-organic framework (MOF) structures have been identified which exhibit a strong adsorptive preference for either *ortho*-xylene (oX)⁵⁻⁹ or pX¹⁰⁻¹¹, providing potential alternatives to existing zeolitic adsorbents.

1
2
3 Since its discovery in 2008, the zirconium-based MOF UiO-66(Zr)¹² has been the subject of a
4 great deal of interest in the scientific community. Comprised of zirconium oxide clusters
5 connected by benzene dicarboxylate (BDC) linkers, the framework demonstrates excellent
6 chemical, hydrothermal and mechanical stability¹²⁻¹³, making it an attractive proposition for
7 many industrial applications, including xylene separations^{4,6}.
8
9

10
11
12
13
14
15 The pore network of UiO-66(Zr) is constructed from larger, octahedral cavities connected by
16 smaller tetrahedral pores (Figure 1). In order to diffuse through the framework, a molecule must
17 pass from one type of pore to the other via a small window of roughly 4 – 5 Å in diameter.
18
19
20
21
22
23
24



25
26
27
28
29
30
31
32
33
34
35
36
37
38
39
40
41
42 Figure 1 - Pore structure of UiO-66(Zr). The dehydroxylated form of the MOF (left) contains
43 octahedral cavities (blue) surrounded by uniformly sized tetrahedral pores (red). In addition to
44 the central octahedral cavity (blue), hydroxylated UiO-66(Zr) contains two distinct tetrahedral
45 pores (red and yellow in the image on the right). Color scheme: C – cyan; H – white; O – red; Zr
46 – grey.
47
48
49
50
51
52
53
54

55 As-synthesized UiO-66 is fully hydroxylated, with each metal cluster containing four hydroxyl
56 groups alongside eight-coordinated zirconium atoms [Zr₆O₄(OH)₄]. Two of these hydroxyl
57
58
59
60

1
2
3 groups along with the remaining two hydrogen atoms can be driven off under heating above
4
5 523 K, producing a de-hydroxylated structure wherein each cluster contains only oxygen and
6
7 seven-coordinated zirconium atoms $[\text{Zr}_6\text{O}_6]^{12}$. In the case of the hydroxylated UiO-66(Zr), the
8
9 presence of $\mu\text{-OH}$ groups results in two distinct types of tetrahedral cavity. The hydroxyl groups
10
11 are located in the slightly larger of the two tetrahedral cavities (~ 7.0 Å in diameter). The slightly
12
13 smaller tetrahedral pores (~ 6.5 Å in diameter) are devoid of hydroxyl groups. The loss of these
14
15 $\mu\text{-OH}$ groups under heating means that only one type of tetrahedral pore (~ 6.6 Å in diameter) is
16
17 present in the de-hydroxylated MOF. The window diameter ($\sim 4\text{-}5$ Å) is the same in both forms
18
19 of UiO-66.
20
21
22
23

24
25 In classical MOF terminology, UiO-66(Zr) is described as being a rigid structure. Even at
26
27 elevated temperature (up to 648 K), the X-ray diffraction (XRD) data reveals no significant
28
29 structural flexibility or breathing effects¹³. Although the MOF does not exhibit any large
30
31 breathing or swelling effects, such as those for example observed in the MIL-53¹⁴ or MIL-88¹⁵
32
33 systems, the structure is not static. In UiO-66(Zr) and its functionalised analogues, the primary
34
35 mode of structural movement is via the rotation or ‘flipping’ of the BDC linker around its long
36
37 axis¹⁶⁻¹⁷. While this linker rotation has little impact on the overall pore size or topology, it has
38
39 been shown to impact considerably on the diffusion of light gases via modulation of the window
40
41 size¹⁸.
42
43
44

45
46 UiO-66 has been shown experimentally to be selective towards $\text{oX}^{4, 6, 19}$, exhibiting so-called
47
48 ‘inverse shape selectivity’, where - in contrast to more conventionally shape selective MOFs
49
50 such as MIL-125(Ti) - oX is favoured over the slimmer pX . In the initial adsorption
51
52 breakthrough studies of Barcia *et al*⁶ and Moreira *et al*⁴, this preference was attributed to the
53
54 close match between the diameters of the pores within the MOF and the kinetic diameter of oX , a
55
56
57
58
59
60

1
2
3 concept previously described in the separation of linear and branched alkanes in the zeolites
4 SAPO-5²⁰ and MCM-22²¹. The least rotationally constrained isomer will experience the lowest
5
6 loss of entropy upon adsorption, resulting in an overall lower Gibbs free energy of adsorption for
7
8 species with similar adsorption enthalpies. In the UiO-66(Zr) – xylene system, this effect is
9
10 expected to manifest itself in an entropic preference for the more compact *ortho*- isomer. This
11
12 entropic driving force has also been held responsible for the experimentally observed preference
13
14 of UiO-66(Zr) for branched over linear C₆ isomers^{6, 22-23}. More recently, Chang and Yan¹⁹ and
15
16 Duerinck *et al*²³ have demonstrated experimentally an additional enthalpic preference for *ortho*-
17
18 xylene, reporting an increased heat of adsorption for oX when compared to mX and pX of 7.5-
19
20 13.1 kJ/mol, which was suggested to be a result of either favorable interactions between the
21
22 aromatic rings of oX and the BDC linkers (π - π stacking) or enhanced electrostatic interactions
23
24 between oX and the μ -OH groups of the MOF.
25
26
27
28
29
30

31
32 While the preliminary computational work of Granato *et al*²⁴ correctly predicted the *ortho*-
33
34 selective nature of the MOF and provided reasonable qualitative agreement for measured
35
36 quantities such as maximum capacity and adsorption enthalpy, the adsorption mechanism and
37
38 origin of the *ortho*-preference remains unclear. This work, therefore, addresses the fundamental
39
40 aspects of xylene adsorption and diffusion in UiO-66(Zr) using a range of computational tools
41
42 and sets out to identify the structural, thermodynamic and kinetic factors which drive the
43
44 experimentally observed *ortho*-selectivity.
45
46
47

48 49 SIMULATION DETAILS

50
51 Both the hydroxylated and de-hydroxylated forms of UiO-66(Zr) were considered in this work.
52
53 The geometry optimized structures of Yang *et al*, which have been shown to successfully
54
55 reproduce light gas adsorption isotherms^{18, 25}, were used. Lennard-Jones parameters for the
56
57
58
59
60

1
2
3 framework atoms were taken from the DREIDING force field²⁶ except in the case of zirconium,
4 which is not included in the DREIDING force field and whose parameters were taken from the
5 UFF²⁷. Partial charges for the MOFs were calculated following the methods of Yang and co-
6 workers²⁸. Xylene isomers were treated as rigid molecules with all atoms defined explicitly with
7 the exception of methyl groups, which were treated as single spheres. The Lennard-Jones
8 parameters and partial charges were taken from the OPLS force field²⁹, which has been shown to
9 capture the behavior of xylenes in UiO-66(Zr) well²⁴.

10
11 The adsorption of xylene isomers in UiO-66(Zr) was simulated at 300 K via grand canonical
12 Monte Carlo (GCMC) simulations implemented in the MuSiC software³⁰. Xylene molecules
13 were subject to energy-biased insertion and deletion, translation and rotation moves. In the case
14 of mixture simulations, identity swap moves were also included. Single component adsorption
15 isotherms were allowed at least 8×10^6 equilibrium steps, followed by 12×10^6 production steps
16 for each pressure point, carefully ensuring that equilibrium was reached before starting the
17 sampling process. Mixture simulations were allowed at least 100×10^6 steps to come to
18 equilibrium, followed by a further 150×10^6 production steps.

19
20 The average interaction energy of the different xylene isomers with the framework in each of
21 the pore types in UiO-66(Zr) was studied through Monte Carlo simulations in the NVT
22 ensemble. Simulations were carried with a total of at least 108 xylene molecules (corresponding
23 to one molecule per cavity of interest) and consisted of at least 8×10^6 equilibrium steps,
24 followed by 12×10^6 production steps. In these simulations, xylene molecules were subjected to
25 random rotation and displacement moves. The starting positions of the xylene molecules were
26 restricted and any displacement which resulted in the center of mass of the molecule entering a
27 neighboring pore was rejected so as only one pore type was explored in each run. The MOF
28
29
30
31
32
33
34
35
36
37
38
39
40
41
42
43
44
45
46
47
48
49
50
51
52
53
54
55
56
57
58
59
60

1
2
3 structures were considered to be rigid and atoms were kept fixed at their optimized
4
5 crystallographic positions in all NVT and μ VT Monte Carlo simulations.
6
7

8 The diffusion of xylene isomers in de-hydroxylated UiO-66(Zr) was studied through molecular
9
10 dynamics (MD) simulations using the DL_Poly Classic package³¹. Initial simulations were
11
12 carried out with the framework held rigid and the atoms kept fixed in their optimized
13
14 crystallographic positions for xylene loadings of 3, 6, 9 and 12 molecules/unit cell (uc). In order
15
16 to assess the impact of framework flexibility on diffusion, further simulations for a xylene
17
18 loading of 3 molecules/uc were carried out in which the movement of MOF atoms was described
19
20 using the force field of Yang and co-workers, which has been shown to replicate well the unit
21
22 cell parameters and equilibrium bond lengths and angles of UiO-66^{18, 25}. Both sets of simulations
23
24 were carried out in the NVT ensemble using a time step of 1 fs. The simulations were allowed at
25
26 least 0.1 ns to equilibrate before a production run of 10 ns. In the rigid MOF, simulations were
27
28 carried out at both 300 K and 500 K, while in the flexible MOF, simulations were undertaken at
29
30 300 K and at temperatures ranging from 500 – 900 K. In both cases, the Berendsen thermostat
31
32 was used to control the temperature. The starting positions of the xylene molecules were taken
33
34 from fully equilibrated GCMC simulations at the appropriate loading.
35
36
37
38
39

40 41 42 RESULTS AND DISCUSSION 43

44 In line with published experimental data^{4, 6}, GCMC simulations of binary xylene mixtures
45
46 show that both de-hydroxylated and hydroxylated forms of UiO-66(Zr) are strongly oX-
47
48 selective, particularly at low partial pressures (Table 1). While the behaviour of oX-mX mixtures
49
50 was found to be largely unaffected by the hydroxylation state of the framework, a marked
51
52 difference in behaviours for mixtures containing pX was observed. Selectivities in pX-containing
53
54 mixtures exhibited a shift towards pX in the hydroxylated MOF: the hydroxylated MOF was
55
56
57
58
59
60

much less selective towards oX for oX-pX mixtures and while the de-hydroxylated MOF was unable to differentiate between pX and mX (i.e. the selectivity is around 1), the hydroxylated MOF was slightly pX-selective in pX-mX mixture simulations.

Table 1 – Simulated selectivity towards species *a* from equimolar binary mixture *a-b* at 1 Pa and 2 kPa in the hydroxylated and de-hydroxylated forms of UiO-66(Zr).

UiO-66(Zr)	oX-mX		oX-pX		pX-mX	
	1 Pa	2 kPa	1 Pa	2 kPa	1 Pa	2 kPa
Hydroxylated	10.4 ± 0.1	7.1 ± 0.1	9.4 ± 0.1	2.3 ± 0.1	1.6 ± 0.2	3.1 ± 0.1
De-hydroxylated	10.1 ± 0.1	6.4 ± 0.1	12.8 ± 0.1	7.0 ± 0.1	1.1 ± 0.2	1.2 ± 0.3

Examination of the simulated single-component isotherms (Figure 2) reveals that the uptake of pX in the hydroxylated MOF is considerably higher than the other two isomers. This is a result of the larger tetrahedral cavity (which is only present in the hydroxylated form of the MOF) being able to accommodate two pX molecules in GCMC simulations, compared to only a single oX or mX molecule (see Figure S2). While the formation of a pX dimer is geometrically possible in this cavity, it is extremely unlikely that it is accessible in reality, where diffusional limitations will prevent a second pX molecule from entering the cavity should the cavity already be occupied. Given that there is no experimental evidence to indicate an enhanced uptake of pX compared to the other two isomers, this phenomenon is likely to be an artefact introduced by the GCMC simulation technique. (Note that while our simulations mimic pure component vapor phase adsorption or liquid phase adsorption from a non-adsorbing solvent, the available experimental data is either competitive xylene adsorption at elevated temperature⁶ or pseudo-single component from a co-adsorbing solvent⁴ and a direct comparison is therefore not

possible). While dimer formation of only one of the isomers would lead to an enhanced selectivity and may be a suitable search criteria for adsorbents with improved performance for xylene separations, further analysis in this work will focus on the de-hydroxylated MOF, where the pX dimer is not observed in simulation and the simulation results are free from this unphysical skew towards pX.

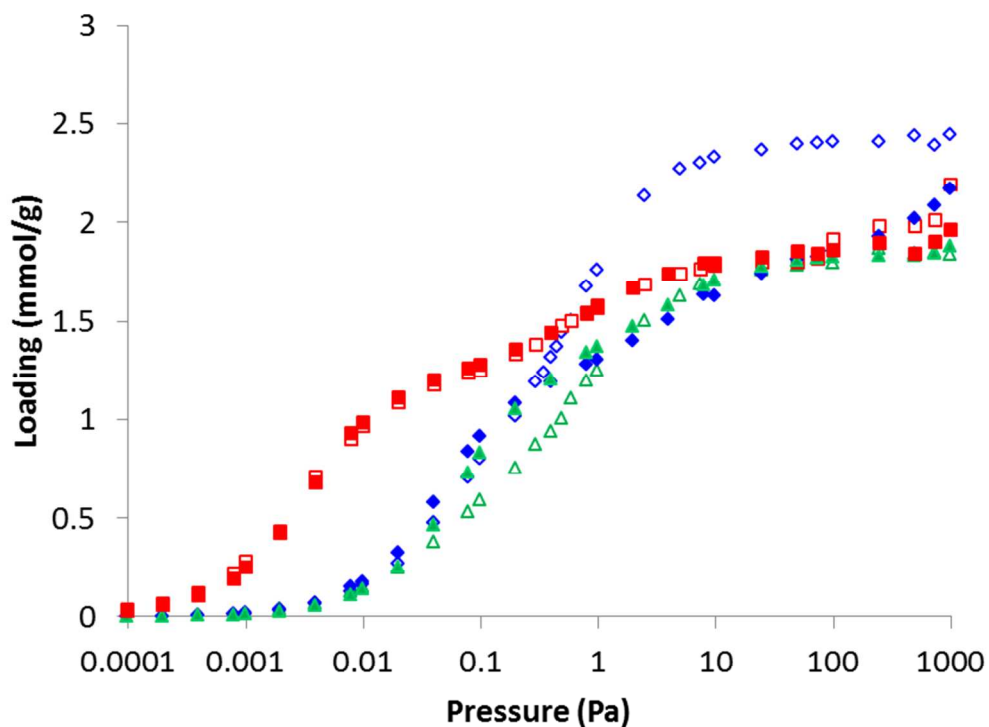


Figure 2 - Simulated single-component isotherms of pX (blue), mX (green) and oX (red) in de-hydroxylated UiO-66(Zr) at 300 K (solid symbols) and in hydroxylated UiO-66(Zr) (empty symbols).

Commensurate with the high oX-selectivity observed in binary GCMC simulations, the low pressure uptake of oX in single-component isotherms is considerably enhanced compared to the other two isomers, which is in qualitative agreement with the experimental work of Moreira *et al*

1
2
3
4
5
6
7
8
9
10
11
12
13
14
15
16
17
18
19
20
21
22
23
24
25
26
27
28
29
30
31
32
33
34
35
36
37
38
39
40
41
42
43
44
45
46
47
48
49
50
51
52
53
54
55
56
57
58
59
60

4. The isotherms of pX and mX in de-hydroxylated UiO-66(Zr) are very similar, exhibiting almost identical uptakes across the full pressure range studied. At low loading, xylene molecules were found to be localized almost exclusively in the tetrahedral cavities of the MOF, in which oX-framework interactions are significantly enhanced compared to pX and mX (6-7 kJ/mol stronger; Figure 3), in agreement with the higher enthalpy of adsorption reported in literature for oX^{19, 23}. In addition, the more compact oX isomer can explore these cavities more easily, with almost 1.5 times the number of accessible adsorption locations within the pore compared to mX and pX (see SI). Thus, the high uptake of oX at low pressure and the strong preference of the MOF for oX in competitive adsorption is a result of a strong energetic preference combined with a non-negligible entropic driving force.

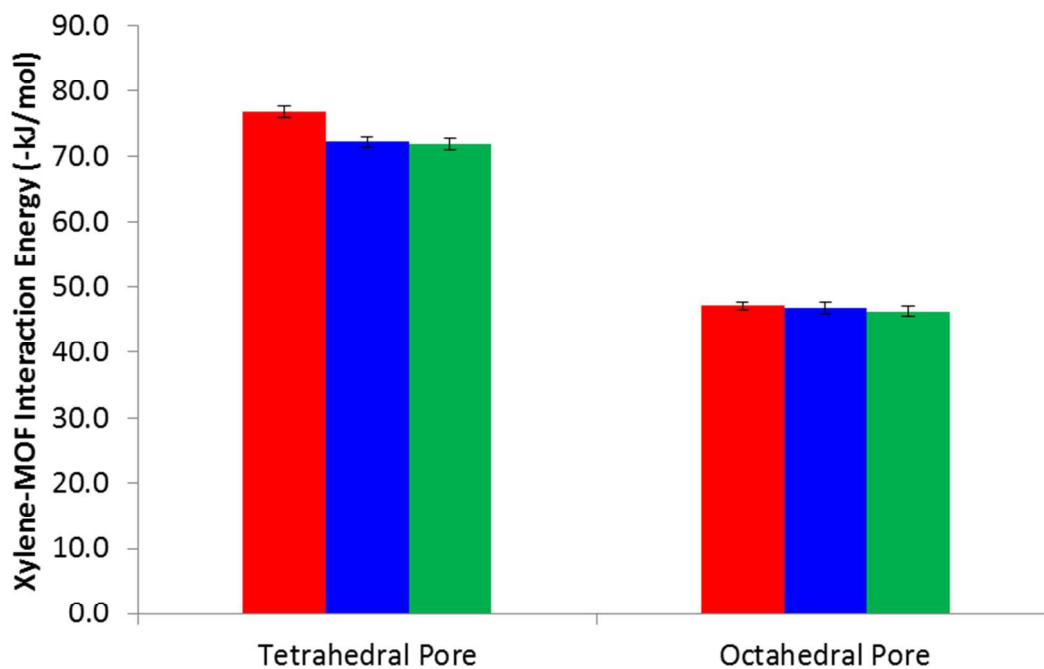


Figure 3 – Xylene-MOF interaction energies calculated per pore in the de-hydroxylated form from NVT MC simulations in the smaller, tetrahedral cavity (diameter 6.6 Å) and larger, octahedral cavity (diameter 7.5 Å) for oX (red), pX (blue) and mX (green).

1
2
3 The electrostatic contribution to the xylene-framework interaction in the tetrahedral pore types
4 was found to be slightly repulsive and of a similar magnitude for all isomers (+0.25 to
5 +1.5 kJ/mol), indicating that van der Waals interactions are responsible for the increase in oX-
6 UiO-66(Zr) interaction energy. Examination of simulation snapshots shows that the origin of this
7 enhancement lies in the ability of oX to position both methyl groups relatively centrally in the
8 pore, allowing a strong interaction with the BDC linkers (Figure 4). In the case of both pX and
9 mX, one or both of the methyl groups are forced away from the center of the pore towards the
10 less energetically favorable pore window – that is, the methyl groups of pX and mX are
11 interacting strongly with only a few framework atoms within the pore window and relatively
12 weakly with the rest of the framework atoms which define the tetrahedral cavity, whereas those
13 of oX are interacting relatively strongly with all six surrounding BDC ligands.
14
15
16
17
18
19
20
21
22
23
24
25
26
27
28
29
30
31
32
33
34
35
36
37
38
39
40
41
42
43
44
45
46
47
48
49
50
51
52
53
54
55
56
57
58
59
60

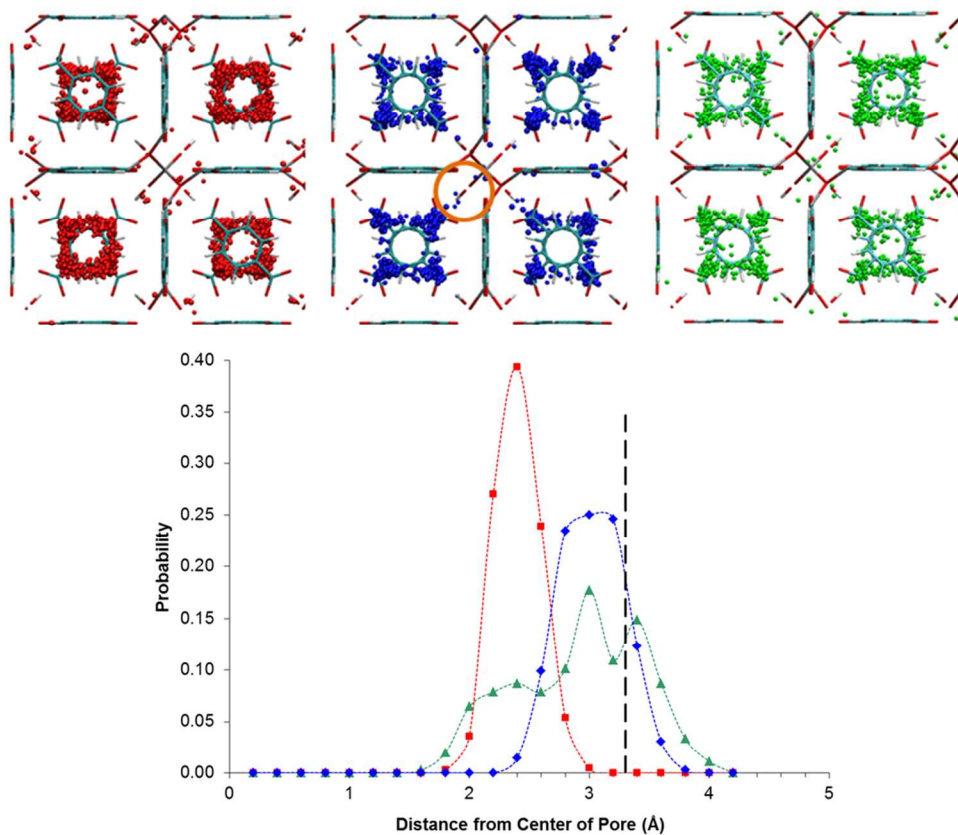


Figure 4 - Top: Observed locations of the methyl groups of oX (red), pX (blue) and mX (green) within UiO-66(Zr) in single component adsorption at 1 Pa. Each dot represents the position of a methyl group over the duration of the simulation. The pore windows are located towards the corners of each pore (e.g. the orange circle in the centre image). Bottom: Corresponding number probability distribution of the methyl groups as a function of radial distance from the centre of the tetrahedral cavity. Lines have been added to guide the eye. The radius of the tetrahedral pore is indicated by the black, dashed line.

None of the snapshots revealed any evidence of xylene molecules taking up a position parallel to one of the BDC linkers, indicating that π - π interactions do not play a significant role in the low-pressure adsorption properties for any of the isomers. Further investigation using a modified version of the Kh_d toolset³² showed that while none of the isomers are sterically restricted from

1
2
3 accessing orientations which allow π - π interactions with the framework, these orientations are
4 not energetically favorable, resulting in much lower xylene-MOF interaction energies (see
5 Supporting Information).
6
7
8
9

10 While the strong preference for *ortho*-xylene observed in vapor-phase quaternary breakthrough
11 experiments⁶ and both liquid-phase binary and ternary breakthrough experiments⁴ is correctly
12 predicted in the present work, the situation is less clear in the case of pX-mX mixtures. In the
13 vapor-phase work of Barcia *et al*⁶, the MOF was unable to discriminate between mX and pX. In
14 the later work of Moreira *et al*⁴, however, UiO-66(Zr) was found to be weakly selective towards
15 mX in both binary mX/pX and ternary oX/mX/pX breakthrough ($S_{\text{pX-mX}} = 0.9$). It should be
16 noted that the studies of Moreira *et al*⁴ were carried out in the liquid phase with heptane as a
17 solvent which results in competitive adsorption of heptane and the xylene isomers. A direct
18 comparison with the simulation is therefore difficult. In the quaternary (pX-mX-oX-
19 ethylbenzene) competitive simulations reported by Granato *et al*²⁴, the MOF exhibited a slight
20 preference for either pX or mX, depending on which force field was selected to describe the
21 xylene isomers. In the present work, the MOF was found to be essentially non-selective (Figure
22 2).
23
24
25
26
27
28
29
30
31
32
33
34
35
36
37
38
39
40

41 The inability of the MOF to discriminate between pX and mX at equilibrium is a direct result
42 of the almost identical xylene-MOF interaction energies for pX and mX in both types of cavity
43 present in UiO-66(Zr) (Figure 3), suggesting that the mX-selectivity observed experimentally is
44 unlikely to be enthalpic in nature. In order to fully understand the selectivity of UiO-66(Zr) for
45 oX and the behavior of the pX-mX mixture observed in breakthrough experiments^{4, 6, 19}, it is
46 necessary to assess the adsorption kinetics and diffusivity of the three isomers in the MOF.
47
48
49
50
51
52
53
54
55
56
57
58
59
60

1
2
3 pore window diameter in the static MOF (4-5 Å) is too small to permit the passage of xylene
4 molecules (the kinetic diameter of the slimmest isomer, pX, is 6.7 Å) and that some degree of
5 structural flexibility is required to enable xylene molecules to diffuse through the MOF. In order
6 to address these points, molecular dynamics (MD) simulations were undertaken in both rigid and
7 flexible UiO-66(Zr), allowing both the underlying diffusion mechanism to be identified and the
8 relative mobility of the three isomers to be assessed.

9
10
11 In MD simulations in which the MOF is kept rigid, none of the xylene isomers were observed
12 moving from one pore to the next, either at 300 K or 500 K. Even in MD simulations in
13 UiO-66(Zr) at 300 K using a force field which allows framework flexibility, xylene molecules
14 remained localized within their starting cages and no transitions between cavities were observed.
15
16 The movement of xylene isomers between cages was only observed in MD simulations
17 undertaken at elevated temperatures (500 – 1000 K), from which we are able to qualitatively
18 explain both the structural movements which facilitate xylene diffusion and the significant
19 differences in transition rate and mechanism between the three isomers.

20
21
22 The window connecting adjoining pores is defined by three BDC linkers arranged in a
23 triangular fashion (Figure 5; left) which, when held rigid, create a hexagonal window with an
24 incircle diameter of ~4-5 Å. When the framework is treated as flexible, the window-defining
25 BDC linkers are able to undergo a rotation around the (OOC)-(COO) axis and twisting and
26 buckling of the aromatic-substituent improper torsion center (Figure 5). The combination of
27 these two motions, induced by interaction between the linkers and adsorbed xylene molecules,
28 causes the window to enlarge and change shape (Figure 5; right), allowing the xylene molecule
29 to move from one pore to the next.
30
31
32
33
34
35
36
37
38
39
40
41
42
43
44
45
46
47
48
49
50
51
52
53
54
55
56
57
58
59
60

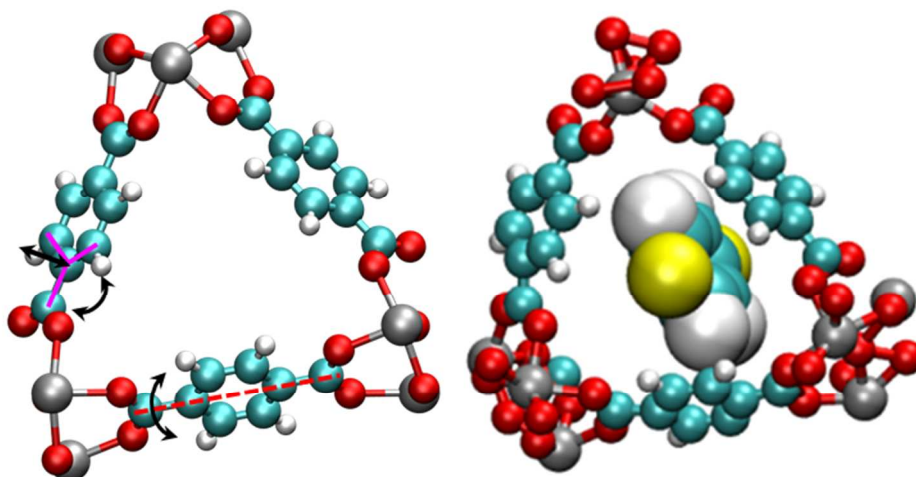


Figure 5 - BDC linkers forming the window present in UiO-66(Zr) in the equilibrium atomic positions used in the rigid structure (left) and during deformation of the window in the presence of pX in MD simulations using a flexible force field (right). The important rotation axis (red dashed line) and torsion center (pink solid lines) are highlighted. Color scheme: C – cyan; H – white; O – red; Zr – grey; CH₃ group – yellow.

In the case of pX and mX, xylene molecules were seen to move between cage types at temperatures of 500 K and above (Figure 6). This transition remained extremely rare at 500 K, with each pX molecule undergoing an average of 0.11 transitions per nanosecond. As the temperature was increased, the transition rate increased to 1.13 molecule⁻¹ ns⁻¹ and 1.52 molecule⁻¹ ns⁻¹ at 800 K and 900 K respectively. mX was found to be much less mobile than pX, with an observed transition rate of 0.02 molecule⁻¹ ns⁻¹ at 500 K – a factor of six lower than pX. oX was found to be the least mobile of the three isomers and transitions were only observed above 800 K.

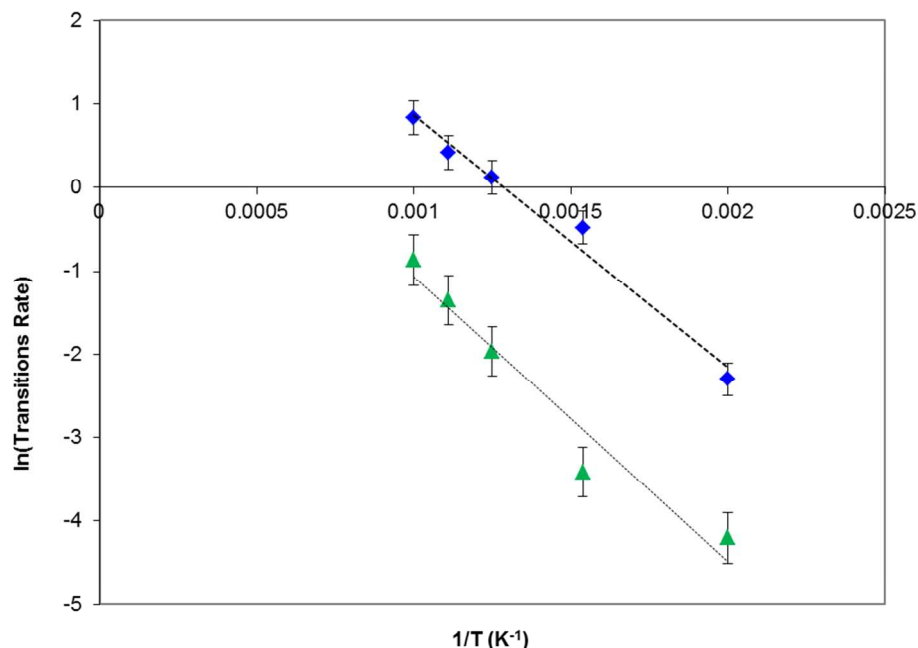


Figure 6 - Temperature-dependence of the cage-to-cage transition rate of pX (blue) and mX (green) in flexible UiO-66(Zr). Dotted lines are those of best fit for determination of Arrhenius coefficients.

The increase in the pX and mX transition rate constant with temperature is well described by the standard Arrhenius equation, from which the activation energy associated with the movement of molecules between cages at low loading was calculated to be 25.2 ± 0.5 kJ/mol for pX and 28.4 ± 1.4 kJ/mol for mX. In contrast to pX and mX, the movement of oX from cage to cage remained an extremely rare event even at elevated temperature. For oX, only two transition events were observed per 10 ns simulation run at 800 K, and only three at 900 K. While it is impossible to accurately determine activation energies from this data, the two order of magnitude difference in transition rate between pX and oX suggests that the activation energy for oX is approximately 20 kJ/mol higher.

1
2
3 Surprisingly, the overall order of mobility observed in MD simulations ($pX > mX \gg oX$) does
4 not correspond to the order of kinetic diameters of the isomers ($pX < oX < mX$). The reason for
5 this apparent discrepancy lies in the fact that the kinetic diameter does not take into account the
6 rotation of the molecule during the transition event. pX was seen to move through the window
7 with minimal rotation of the isomer – the only observed rotation was around the long ($\text{CH}_3\text{-CH}_3$)
8 axis of the molecule (Figure 7; top). The required window diameter (critical diameter) for this
9 motion is approximately 6.7 Å. While moving through the pore window, mX follows a different
10 path, experiencing rotation around the center of the aromatic ring, perpendicular to the long axis
11 of the molecule (Figure 7; middle). As a result of the rotation of the molecule, the critical
12 diameter is much less than the measured kinetic diameter (7.4 Å compared to 7.8 Å). The lower
13 mobility of mX compared to pX is thus primarily a result of the larger critical diameter and the
14 increased distortion of the framework required to allow passage through the window.
15
16
17
18
19
20
21
22
23
24
25
26
27
28
29
30
31
32
33
34
35
36
37
38
39
40
41
42
43
44
45
46
47
48
49
50
51
52
53
54
55
56
57
58
59
60

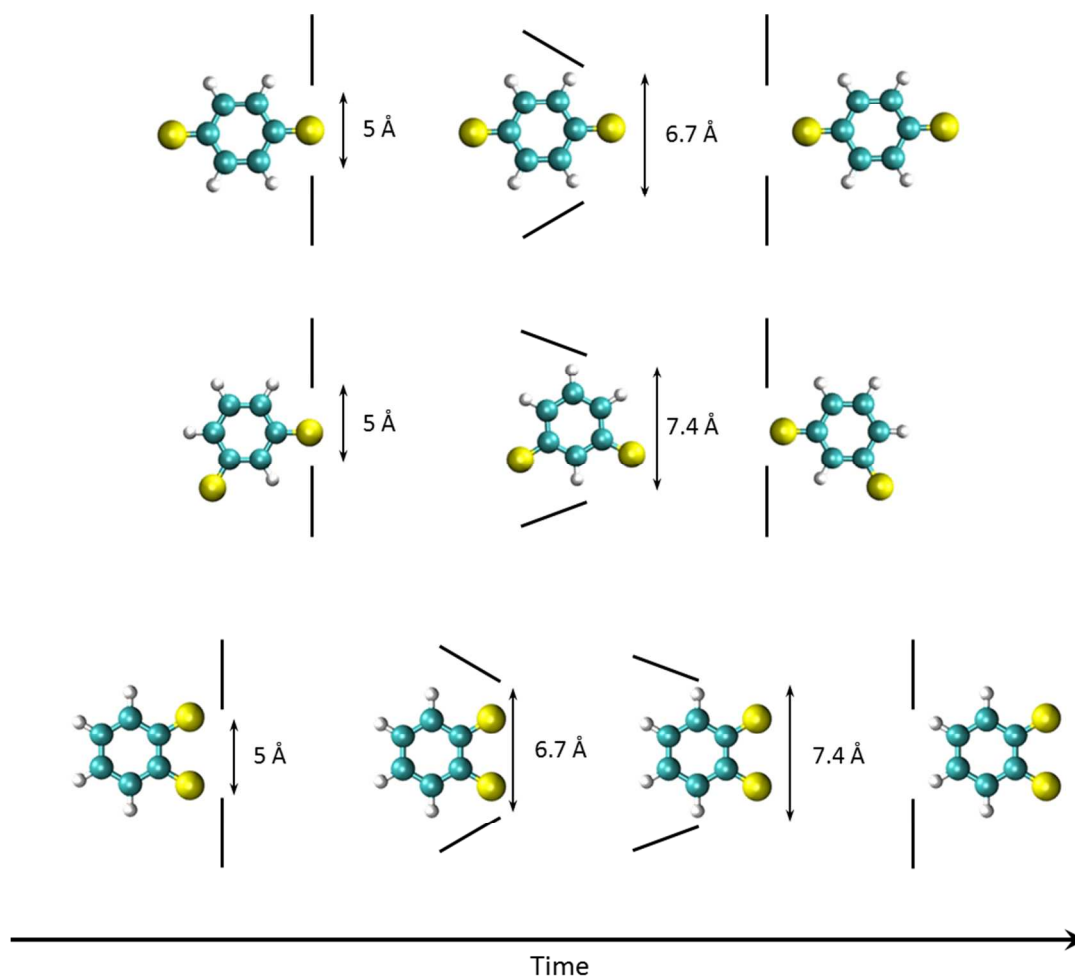


Figure 7 – Schematic representation of the movement of pX (top), mX (middle) and oX (bottom) through the window of UiO-66(Zr). The relative orientation of the linkers is shown by the solid black lines while the minimum window diameter for each of the steps is indicated alongside. Vertical black lines correspond to the equilibrium linker orientation. Color scheme: C – cyan; H – white; CH₃ group – yellow.

The smallest critical diameter which oX is capable of presenting is also 7.4 Å and, given that the window is capable of admitting mX, the movement of oX should not be restricted from a geometric perspective. The primary difference between oX and the other isomers is that the two methyl groups are adjacent, existing as a pair rather than single protruding entities. The pore

1
2
3 window has an equilibrium diameter of roughly 4 - 5 Å, while the single methyl group has a
4
5 diameter of 3.8 Å in these simulations. It is clear that even without framework distortion the
6
7 single methyl group is able to enter the pore window. In contrast, the methyl pair on oX has a
8
9 combined diameter of approximately 6.7 Å – too large to enter into the pore window without
10
11 prior distortion of the framework (Figure 7; bottom).
12
13

14
15 The single methyl groups present on mX and pX thus act as a wedge whose presence within
16
17 the pore window is able to induce further distortion of the framework, enlarging the window and
18
19 enabling the rest of the molecule to pass through. The low mobility of oX is therefore a result of
20
21 the molecule being forced to wait for the window to spontaneously enlarge before any portion of
22
23 the molecule is able to enter the window. The ability of pX and mX to position their methyl
24
25 groups within the pore windows even when the structure is at equilibrium is supported by the
26
27 GCMC results presented earlier, wherein both pX and mX were observed to preferentially locate
28
29 one or both methyl groups in the pore window (Figure 4). In GCMC simulations, this had the
30
31 effect of reducing the adsorption affinity of the MOF for pX and mX compared to oX. The
32
33 complete encapsulation of the oX molecule within the pore thus enhances the equilibrium
34
35 selectivity, while simultaneously reducing the mobility of oX within the framework compared to
36
37 pX and mX, introducing an additional kinetic selectivity to the system. The breakthrough
38
39 experiments of Moreira *et al*⁴ provide some evidence of a considerably lower transition rate of
40
41 oX compared to the other two isomers, with oX demonstrating noticeably more disperse
42
43 breakthrough profiles than those of pX and mX. While ethylbenzene (EB) was not considered in
44
45 the present work, it may be expected that the ethyl group – being similarly sterically unhindered
46
47 – would allow it to follow a similar transition mechanism to pX and mX, evidenced in the sharp
48
49 peaks for pX, mX and EB observed in the vapor-phase work of Barcia *et al*⁶. Furthermore, one
50
51
52
53
54
55
56
57
58
59
60

1
2
3 may expect that while the longer alkyl group in EB may prevent the molecule from being as well
4 encapsulated as oX, the additional configurational freedom experienced by EB compared to the
5
6 other isomers may play a significant role and future work should seek to explore these aspects of
7
8 the behavior of EB within UiO-66. Additionally it is important to note, however, that the UiO-66
9
10 system has been shown to be susceptible to missing linker defect formation³³⁻³⁴ and further work
11
12 is required to quantify the influence of these defects on xylene adsorption and diffusion.
13
14
15
16
17

18 CONCLUSIONS

19
20
21 In this work, we carried out a detailed computational study of the unusual behavior of xylene
22 isomers in the metal-organic framework UiO-66(Zr), augmenting GCMC simulations of
23 adsorption with NVT MC, complementary geometric tools and MD simulations in both rigid and
24 flexible models of the framework. We demonstrate that such a combined computational
25 approach is required to fully understand the previously reported selectivity of the MOF for oX –
26 shown here to be strongly dependent on both the equilibrium and kinetic properties of the
27 xylene-MOF system.
28
29
30
31
32
33
34
35
36
37

38 The clear preference of the MOF for oX observed in experiment was correctly predicted by
39 simulation and, furthermore, the calculated xylene-framework interactions are in good agreement
40 with the enthalpies of adsorption determined experimentally^{19, 23}. It was shown that the enhanced
41 xylene-framework interactions observed for oX in comparison to the other two isomers arises
42 from neither π - π nor electrostatic interactions but is a result of the complete encapsulation of the
43 oX molecule within the tetrahedral cavities. Geometric restrictions force the other isomers to
44 take up less energetically favorable positions with one or both methyl groups located in the pore
45 windows.
46
47
48
49
50
51
52
53
54
55
56
57
58
59
60

1
2
3 While xylene adsorption in UiO-66(Zr) was well-predicted when the framework is kept rigid
4 (not exhibiting any large scale breathing behavior or gate opening effects, UiO-66 is considered
5 to be a rigid MOF), the flexibility of the MOF and movement of atoms away from their
6 crystallographic positions was found to be crucial in allowing xylene molecules to diffuse
7 through the structure. The movement of xylene molecules from one cage to the next was only
8 observed during simulations using a flexible framework. The ability of the BDC linkers to both
9 rotate and flex in response to interaction with adsorbed xylene molecules was seen to result in an
10 enlargement of the window diameter, enabling xylenes to pass from one pore to the next. This
11 transition was found to be hindered considerably in the case of oX, whose adjacent methyl
12 groups are less able to induce the enlargement of the window than the individual methyl groups
13 of pX and mX. The overall high oX-selectivity observed in breakthrough experiment is therefore
14 a combination of both a kinetic contribution and the previously established enthalpic preference.
15 The higher activation energy for the movement of mX through the pore network when compared
16 to pX, combined with the lack of clear preference for either component in GCMC simulations,
17 suggests that the slight selectivity towards mX observed in some experiments is also kinetic
18 rather than enthalpic in nature.
19
20
21
22
23
24
25
26
27
28
29
30
31
32
33
34
35
36
37
38
39

40 While the present work highlights the key role which computational techniques have to play in
41 identifying the structural features integral to adsorption-based xylene separations, the strong
42 influence of framework flexibility on xylene behavior reported herein – and recently
43 demonstrated for the similarly ‘rigid’ MIL-47 and MOF-48 systems³⁵ – provides further
44 evidence that the incorporation of flexibility in molecular simulation must be addressed when
45 screening MOFs computationally for industrial adsorption applications.
46
47
48
49
50
51
52
53
54

55
56 SUPPORTING INFORMATION
57
58
59
60

1
2
3 Pore size distributions for hydroxylated and dehydroxylated UiO-66(Zr); pX dimer formation
4
5 in hydroxylated UiO-66(Zr); calculation of the accessible adsorption sites for the three isomers,
6
7
8 additional simulation details of evaluation of π - π stacking of xylenes in UiO-66(Zr).
9

10 11 ACKNOWLEDGMENTS

12
13
14 The research leading to these results has received funding from the European Community's
15
16 Seventh Framework Programme (FP7/2007-2013) under grant agreement No. 228862. This work
17
18 has made use of the resources provided by the Edinburgh Compute and Data Facility (ECDF)
19
20 (<http://www.ecdf.ed.ac.uk/>). The authors wish to thank Prof. Guillaume Maurin and Dr.
21
22 Qingyuan Yang for providing the structure and partial atomic charges for hydroxylated UiO-
23
24 66(Zr) and Dr. Naseem Ramsahye for guidance on the implementation of MD simulations in
25
26 flexible UiO-66(Zr) in DL_POLY.
27
28
29
30

31 32 AUTHOR INFORMATION

33
34
35 The authors confirm that the manuscript through contributions from all authors and declare no
36
37 competing financial interest.
38
39

40
41 *Corresponding author: T.Duren@bath.ac.uk
42

43 44 REFERENCES

- 45
46
47 1. Sholl, D. S.; Lively, R. P., Seven Chemical Separations to Change the World. *Nature* **2016**, *532*,
48 435-437.
49 2. Cannella, W. J., Xylenes and Ethylbenzene. In *Kirk-Othmer Encyclopedia of Chemical Technology*,
50 John Wiley & Sons, Inc.: 2000.
51 3. Kurup, A. S.; Hidajat, K.; Ray, A. K., Optimal Operation of an Industrial-Scale Parex Process for the
52 Recovery of P-Xylene from a Mixture of C-8 Aromatics. *Industrial & Engineering Chemistry Research*
53 **2005**, *44*, 5703-5714.
54 4. Moreira, M. A., et al., Reverse Shape Selectivity in the Liquid-Phase Adsorption of Xylene
55 Isomers in Zirconium Terephthalate Mof UiO-66. *Langmuir* **2012**, *28*, 5715-5723.
56
57
58
59
60

5. Alaerts, L.; Maes, M.; Giebeler, L.; Jacobs, P. A.; Martens, J. A.; Denayer, J. F. M.; Kirschhock, C. E. A.; De Vos, D. E., Selective Adsorption and Separation of Ortho-Substituted Alkylaromatics with the Microporous Aluminum Terephthalate Mil-53. *J. Am. Chem. Soc.* **2008**, *130*, 14170-14178.
6. Barcia, P. S.; Guimaraes, D.; Mendes, P. A. P.; Silva, J. A. C.; Guillerm, V.; Chevreau, H.; Serre, C.; Rodrigues, A. E., Reverse Shape Selectivity in the Adsorption of Hexane and Xylene Isomers in Mof Uio-66. *Microporous and Mesoporous Materials* **2011**, *139*, 67-73.
7. El Osta, R.; Carlin-Sinclair, A.; Guillou, N.; Walton, R. I.; Vermoortele, F.; Maes, M.; de Vos, D.; Millange, F., Liquid-Phase Adsorption and Separation of Xylene Isomers by the Flexible Porous Metal-Organic Framework Mil-53(Fe). *Chem. Mat.* **2012**, *24*, 2781-2791.
8. Gu, Z.-Y.; Jiang, D.-Q.; Wang, H.-F.; Cui, X.-Y.; Yan, X.-P., Adsorption and Separation of Xylene Isomers and Ethylbenzene on Two Zn-Terephthalate Metal-Organic Frameworks. *The Journal of Physical Chemistry C* **2009**, *114*, 311-316.
9. Trens, P.; Belarbi, H.; Shepherd, C.; Gonzalez, P.; Ramsahye, N. A.; Lee, U. H.; Seo, Y. K.; Chang, J. S., Adsorption and Separation of Xylene Isomers Vapors onto the Chromium Terephthalate-Based Porous Material Mil-101(Cr): An Experimental and Computational Study. *Microporous and Mesoporous Materials* **2014**, *183*, 17-22.
10. Vermoortele, F., et al., P-Xylene-Selective Metal-Organic Frameworks: A Case of Topology-Directed Selectivity. *J. Am. Chem. Soc.* **2011**, *133*, 18526-18529.
11. Gee, J. A.; Zhang, K.; Bhattacharyya, S.; Bentley, J.; Rungta, M.; Abichandani, J. S.; Sholl, D. S.; Nair, S., Computational Identification and Experimental Evaluation of Metal-Organic Frameworks for Xylene Enrichment. *The Journal of Physical Chemistry C* **2016**.
12. Cavka, J. H.; Jakobsen, S.; Olsbye, U.; Guillou, N.; Lamberti, C.; Bordiga, S.; Lillerud, K. P., A New Zirconium Inorganic Building Brick Forming Metal Organic Frameworks with Exceptional Stability. *J. Am. Chem. Soc.* **2008**, *130*, 13850-13851.
13. Valenzano, L.; Civalieri, B.; Chavan, S.; Bordiga, S.; Nilsen, M. H.; Jakobsen, S.; Lillerud, K. P.; Lamberti, C., Disclosing the Complex Structure of Uio-66 Metal Organic Framework: A Synergic Combination of Experiment and Theory. *Chem. Mat.* **2011**, *23*, 1700-1718.
14. Serre, C.; Millange, F.; Thouvenot, C.; Nogues, M.; Marsolier, G.; Louer, D.; Férey, G., Very Large Breathing Effect in the First Nanoporous Chromium(III)-Based Solids: Mil-53 or Cr-III(OH)Center Dot{O2c-C6h4-Co2}Center Dot{Ho2c-C6h4-Co2h}{X}Center Dot H2Oy. *J. Am. Chem. Soc.* **2002**, *124*, 13519-13526.
15. Serre, C.; Millange, F.; Surblé, S.; Férey, G., A Route to the Synthesis of Trivalent Transition-Metal Porous Carboxylates with Trimeric Secondary Building Units. *Angewandte Chemie International Edition* **2004**, *43*, 6285-6289.
16. Kolokolov, D. I.; Stepanov, A. G.; Guillerm, V.; Serre, C.; Frick, B.; Jovic, H., Probing the Dynamics of the Porous Zr Terephthalate Uio-66 Framework Using H-2 Nmr and Neutron Scattering. *J. Phys. Chem. C* **2012**, *116*, 12131-12136.
17. Devautour-Vinot, S.; Maurin, G.; Serre, C.; Horcajada, P.; da Cunha, D. P.; Guillerm, V.; Costa, E. D.; Taulelle, F.; Martineau, C., Structure and Dynamics of the Functionalized Mof Type Uio-66(Zr): Nmr and Dielectric Relaxation Spectroscopies Coupled with Dft Calculations. *Chem. Mat.* **2012**, *24*, 2168-2177.
18. Yang, Q. Y.; Wiersum, A. D.; Jovic, H.; Guillerm, V.; Serre, C.; Llewellyn, P. L.; Maurin, G., Understanding the Thermodynamic and Kinetic Behavior of the Co2/Ch4 Gas Mixture within the Porous Zirconium Terephthalate Uio-66(Zr): A Joint Experimental and Modeling Approach. *J. Phys. Chem. C* **2011**, *115*, 13768-13774.
19. Chang, N.; Yan, X.-P., Exploring Reverse Shape Selectivity and Molecular Sieving Effect of Metal-Organic Framework Uio-66 Coated Capillary Column for Gas Chromatographic Separation. *Journal of Chromatography A* **2012**, *1257*, 116-124.

- 1
 - 2
 - 3
 - 4
 - 5
 - 6
 - 7
 - 8
 - 9
 - 10
 - 11
 - 12
 - 13
 - 14
 - 15
 - 16
 - 17
 - 18
 - 19
 - 20
 - 21
 - 22
 - 23
 - 24
 - 25
 - 26
 - 27
 - 28
 - 29
 - 30
 - 31
 - 32
 - 33
 - 34
 - 35
 - 36
 - 37
 - 38
 - 39
 - 40
 - 41
 - 42
 - 43
 - 44
 - 45
 - 46
 - 47
 - 48
 - 49
 - 50
 - 51
 - 52
 - 53
 - 54
 - 55
 - 56
 - 57
 - 58
 - 59
 - 60
20. Santilli, D. S.; Harris, T. V.; Zones, S. I., Inverse Shape Selectivity in Molecular Sieves: Observations, Modelling, and Predictions. *Microporous Materials* **1993**, *1*, 329-341.
21. Denayer, J. F. M.; Ocakoglu, R. A.; Arik, I. C.; Kirschhock, C. E. A.; Martens, J. A.; Baron, G. V., Rotational Entropy Driven Separation of Alkane/Isoalkane Mixtures in Zeolite Cages. *Angewandte Chemie International Edition* **2005**, *44*, 400-403.
22. Bozbiyik, B.; Duerinck, T.; Lannoeye, J.; De Vos, D. E.; Baron, G. V.; Denayer, J. F. M., Adsorption and Separation of N-Hexane and Cyclohexane on the Uio-66 Metal-Organic Framework. *Microporous and Mesoporous Materials* **2014**, *183*, 143-149.
23. Duerinck, T.; Bueno-Perez, R.; Vermoortele, F.; De Vos, D. E.; Calero, S.; Baron, G. V.; Denayer, J. F. M., Understanding Hydrocarbon Adsorption in the Uio-66 Metal-Organic Framework: Separation of (Un)Saturated Linear, Branched, Cyclic Adsorbates, Including Stereoisomers. *J. Phys. Chem. C* **2013**, *117*, 12567-12578.
24. Granato, M. A.; Martins, V. D.; Ferreira, A. F. P.; Rodrigues, A. E., Adsorption of Xylene Isomers in Mof Uio-66 by Molecular Simulation. *Microporous and Mesoporous Materials* **2014**, *190*, 165-170.
25. Yang, Q.; Jobic, H.; Salles, F.; Kolokolov, D.; Guillerm, V.; Serre, C.; Maurin, G., Probing the Dynamics of Co₂ and Ch₄ within the Porous Zirconium Terephthalate Uio-66(Zr): A Synergic Combination of Neutron Scattering Measurements and Molecular Simulations. *Chem.-Eur. J.* **2011**, *17*, 8882-8889.
26. Mayo, S. L.; Olafson, B. D.; Goddard, W. A., Dreiding - a Generic Force-Field for Molecular Simulations. *J Phys Chem-US* **1990**, *94*, 8897-8909.
27. Rappe, A. K.; Casewit, C. J.; Colwell, K. S.; Goddard, W. A.; Skiff, W. M., Uff, a Full Periodic-Table Force-Field for Molecular Mechanics and Molecular-Dynamics Simulations. *J. Am. Chem. Soc.* **1992**, *114*, 10024-10035.
28. Yang, Q. Y.; Wiersum, A. D.; Llewellyn, P. L.; Guillerm, V.; Serred, C.; Maurin, G., Functionalizing Porous Zirconium Terephthalate Uio-66(Zr) for Natural Gas Upgrading: A Computational Exploration. *Chem. Commun.* **2011**, *47*, 9603-9605.
29. Jorgensen, W. L.; Laird, E. R.; Nguyen, T. B.; Tiradorives, J., Monte-Carlo Simulations of Pure Liquid Substituted Benzenes with Opls Potential Functions. *Journal of Computational Chemistry* **1993**, *14*, 206-215.
30. Gupta, A.; Chempath, S.; Sanborn, M. J.; Clark, L. A.; Snurr, R. Q., Object-Oriented Programming Paradigms for Molecular Modeling. *Mol. Simul.* **2003**, *29*, 29-46.
31. Todorov, I. T.; Smith, W.; Trachenko, K.; Dove, M. T., DI_Poly_3: New Dimensions in Molecular Dynamics Simulations Via Massive Parallelism. *J. Mater. Chem.* **2006**, *16*, 1911-1918.
32. Sarkisov, L., Toward Rational Design of Metal-Organic Frameworks for Sensing Applications: Efficient Calculation of Adsorption Characteristics in Zero Loading Regime. *J. Phys. Chem. C* **2012**, *116*, 3025-3033.
33. Wu, H.; Chua, Y. S.; Krungleviciute, V.; Tyagi, M.; Chen, P.; Yildirim, T.; Zhou, W., Unusual and Highly Tunable Missing-Linker Defects in Zirconium Metal-Organic Framework Uio-66 and Their Important Effects on Gas Adsorption. *J. Am. Chem. Soc.* **2013**, *135*, 10525-10532.
34. Cliffe, M. J.; Wan, W.; Zou, X.; Chater, P. A.; Kleppe, A. K.; Tucker, M. G.; Wilhelm, H.; Funnell, N. P.; Coudert, F.-X.; Goodwin, A. L., Correlated Defect Nanoregions in a Metal-Organic Framework. *Nat Commun* **2014**, *5*.
35. Gee, J. A.; Sholl, D. S., Effect of Framework Flexibility on C-8 Aromatic Adsorption at High Loadings in Metal-Organic Frameworks. *J. Phys. Chem. C* **2016**, *120*, 370-376.

1
2
3
4
5
6
7
8
9
10
11
12
13
14
15
16
17
18
19
20
21
22
23
24
25
26
27
28
29
30
31
32
33
34
35
36
37
38
39
40
41
42
43
44
45
46
47
48
49
50
51
52
53
54
55
56
57
58
59
60

TOC Graphic

